Geophys. J. Int. (2008) **173,** 766–780 doi: 10.1111/j.1365-246X.2008.03750.x

Fast 3-D simulation of transient electromagnetic fields by model reduction in the frequency domain using Krylov subspace projection

Ralph-Uwe Börner,[1,2] Oliver G. Ernst[1,3] and Klaus Spitzer[1,2]

[1] *Technische Universität Bergakademie Freiberg, Freiberg, Germany. E-mail: rub@geophysik.tu.freiberg.de*
[2] *Institute of Geophysics, Technische Universität Bergakademie Freiberg, Freiberg, Germany*
[3] *Institute of Numerical Analysis and Optimization, Technische Universität Bergakademie Freiberg, Freiberg, Germany*

Accepted 2008 January 31. Received 2007 November 30; in original form 2007 February 7

SUMMARY

We present an efficient numerical method for the simulation of transient electromagnetic fields resulting from magnetic and electric dipole sources in three dimensions.

The method we propose is based on the Fourier synthesis of frequency domain solutions at a sufficient number of discrete frequencies obtained using a finite element (FE) approximation of the damped vector wave equation obtained after Fourier transforming Maxwell's equations in time. We assume the solution to be required only at a few points in the computational domain, whose number is small relative to the number of FE degrees of freedom. The mapping which assigns to each frequency the FE approximation at these points of interest is a vector-valued rational function known as the transfer function. Its evaluation is approximated using Krylov subspace projection, a standard model reduction technique. Computationally, this requires the FE discretization at a small number of reference frequencies and the generation of a sufficiently large Krylov subspace associated with each reference frequency. Once a basis of this subspace is available, a sufficiently accurate rational approximation of the transfer function can be evaluated at the remaining frequencies at negligible cost. These partial frequency domain solutions are then synthesized to the time evolution at the points of interest using a fast Hankel transform.

To test the algorithm, responses obtained by2-D and 3-D FE formulations have been calculated for a layered half-space and compared with results obtained analytically, for which we observed a maximum deviation of less than 2 per cent in the case of transient EM modelling. We complete our model studies with a number of comparisons with established numerical approaches.

A first implementation of our new numerical algorithm already gives very good results using much less computational time compared with time stepping methods and comparable times and accuracy compared with the Spectral Lanczos Decomposition Method (SLDM).

Key words: Numerical solutions; Fourier analysis; Numerical approximations and analysis; Electromagnetic theory; Marine electromagnetics.

1 INTRODUCTION

The transient electromagnetic (TEM) method has become one of the standard techniques in geo-electromagnetism and is now widely used, for example, for exploration of groundwater, mineral and hydrocarbon resources. The numerical computation of TEM fields is of particular interest in applied geophysics. First introduced by Yee (1966), the finite difference time domain (FDTD) technique has been widely used to simulate the transient fields in 2-D and 3-D engineering applications by time stepping (Taflove 1995). In geophysics, first attempts to numerically simulate transients were made by Goldman & Stoyer (1983) for axisymmetric conductivity structures using implicit time-stepping. Wang & Hohmann (1993) have developed an explicit FDTD method in 3-D based on Du Fort-Frankel time-stepping.

Generally, explicit time stepping algorithms require small time steps to maintain numerical stability. For the simulation of late-time responses their computational cost must, therefore, be regarded as very high. Several attempts have been made to reduce the numerical effort, for example, by a special treatment of the air–earth interface to circumvent excessively small time steps due to the extremely low conductivity of the air layer (Oristaglio & Hohmann 1984; Wang & Hohmann 1993). For explicit FDTD methods, it thus seems that acceptable computing times can only be achieved by parallelization using computer clusters (Commer & Newman 2004).

© 2008 The Authors
Journal compilation © 2008 RAS

Downloaded from https://academic.oup.com/gji/article/173/3/766/736358 by U.S. Department of Justice user on 17 August 2022

Implicit time-stepping, while removing the stability constraint on the time step, requires the solution of a large linear system of equations at each time step. While this seems daunting for 3-D problems, recent advances in multigrid methods for the curl–curl operator (Reitzinger & Schoeberl 2002; Aruliah & Ascher 2003; Hiptmair & Xu 2006; Greif & Schötzau 2007) may make this a viable option for TEM.

An alternative approach to time-stepping was proposed by Druskin & Knizhnerman (1988) and has since been known as the Spectral Lanczos Decomposition Method (SLDM). Their original method uses a 3-D finite difference (FD) approximation of Maxwell's equations, which are cast into a system of ordinary differential equations. The solution of the latter is formulated as a multiplication of a matrix exponential with a vector of initial values. Numerical evidence indicates that the convergence of the SLDM depends mainly on the conductivity contrasts within the model. To improve convergence, the FD grids have to be refined near jumps of electrical conductivity within the discretized region. However, the FD tensor product grids further increase the number of unknowns even in regions where densely sampled solutions are not of particular interest, for example, at greater depths. We note, however, that the time-stepping technique that is inherent to SLDM can be combined with other spatial discretizations.

The approach of modelling in the frequency domain with subsequent transformation into the time domain was proposed by Newman *et al.* (1986), who used a 3-D integral equation method to provide the responses for typically 20–40 frequencies, which are transformed into the time domain using a digital filtering technique (Anderson 1979). However, the time domain results displayed deviations from reference solutions at late times due to the limited accuracy of the 3-D responses.

The use of finite element (FE) discretizations for field problems in geophysics dates back at least to Coggon (1971), who obtained solutions to DC problems in 2-D using linear triangular elements and also discussed the issue of placing the outer boundary of the computational domain sufficiently far away from inhomogeneities and sources in order to be able to apply simple homogeneous Dirichlet or Neumann boundary conditions there. This issue was treated by essentially an integral equation boundary condition in (Lee *et al.* 1981; Gupta *et al.* 1987, 1989), who refer to this approach as a 'hybrid' or 'compact FE' scheme. FE approximations for 3-D scalar and vector formulations were also employed by Livelybrooks (1993).

Everett & Edwards (1993) have published a FE discretization for the solution of a 2.5 D problem with subsequent Laplace transform of the response of electric dipoles located on the seafloor. A FE solution of geo-electromagnetic problems for 2-D sources using isoparametric quadratic elements has been introduced by Mitsuhata (2000) with respect to frequency domain modelling of dipole sources over undulating surfaces.

Sugeng *et al.* (1993) have computed the step response solutions for 31 frequencies over a range between 1 and 1000 kHz using isoparametric FEs. The authors report small deviations in the late time response.

One of the difficulties in the numerical modelling of electromagnetic field problems using FE is the possible discontinuity of normal field components across discontinuities of material properties. Standard Lagrange elements, sometimes called 'nodal' elements, which force all field components to be continuous across element boundaries, cannot reproduce these physical phenomena. This difficulty was resolved by the curl-conforming elements of Nédélec (1980, 1986), which are referred to as 'edge elements' in the engineering literature since the lowest order elements of this family carry their degrees of freedom at element edges. The FE subspaces of the Nédélec family perfectly capture the discontinuities of the electric and magnetic fields along material discontinuities. The first application of edge elements to geoelectric problems were probably Jin *et al.* (1999), who developed a frequency-domain and time-domain FE solution using SLDM for a small bandwidth of frequencies and very short times, respectively.

This paper introduces a method based on a FE discretization in the frequency domain. We avoid the heavy computational expense associated with solving a full 3-D problem for each of many frequencies by a model reduction approach. The point of departure is that the transients, which are synthesized from the frequency domain solutions, are required only at a small number of receiver locations. The synthesis of the transients at these locations, therefore, requires only frequency domain solutions at these points. After discretization in space, the frequency domain solution values at the receiver points are rational functions of frequency. Using Krylov subspace projection as a model reduction technique (*cf.* Antoulas 2005) it is possible to approximate this function, known as the 'transfer function' in linear systems theory, by rational functions of lower order. Computationally, the discretized frequency-domain problem for a suitably chosen reference frequency is projected onto a Krylov subspace of low dimension, yielding the desired approximation of the transfer function in terms of quantities generated in the Arnoldi process, which is used to construct an orthonormal basis of the Krylov subspace. This approximation, the evaluation of which incurs only negligible cost, is then used for all the other frequencies needed for the synthesis. While more difficult model reduction problems such as those arising in semiconductor device simulation require repeating this process at several reference frequencies across the spectral bandwidth of interest, our experience has shown the time evolution of the electromagnetic fields after a current shut-off to be a very benign problem for which one or two reference frequencies suffice. After obtaining frequency-domain approximations at the receiver locations for all required frequencies in this way, the associated transients are synthesized using a fast Hankel transform (*cf.* Newman *et al.* 1986). The resulting algorithm thus has as its main expense the FE solution at the reference frequency and the Arnoldi process to construct the Krylov space. Since each Arnoldi step requires the solution of a linear system with the coefficient matrix associated with the reference frequency problem, we generate a sparse LU factorization of this matrix, which we found feasible for problem sizes of up to around 250 000 using the PARDISO software of Schenk & Gärtner (2004). For much larger problems the linear systems can instead be solved iteratively. Our computational experiments demonstrate that the proposed method can, as an example, compute transients at several receiver locations based on a discretization with 100 000 degrees of freedom in roughly 5 min wall clock time on current desktop hardware.

Our method is probably closest to that proposed by Druskin *et al.* (1999). What distinguishes it from theirs, besides the use of a FE discretization in place of FDs, is that we allow for one or more frequency shifts, which, as our numerical examples will show, can dramatically accelerate convergence, whereas the approach of (Druskin *et al.* 1999) corresponds to using a fixed zero shift. Moreover, interpreting our approach in the context of model reduction allows many more sophisticated model reduction techniques to be applied to geo-electromagnetic problems.

We note that solutions to such multiple-frequency partial-field problems have been published by Wagner *et al.* (2003) in the context of an acoustic fluid–structure interaction problem.

Downloaded from https://academic.oup.com/gji/article/173/3/766/736358 by U.S. Department of Justice user on 17 August 2022

The remainder of this paper is organized as follows. Section 3 recalls the governing equations of time-harmonic electromagnetics with a shut-off magnetic dipole source as well as the mappings between time and frequency domains. In Section 4, we derive the weak formulation of the resulting boundary value problem for the electric field and present the FE discretization using tetrahedral Nédélec elements. Our proposed Krylov subspace-based model reduction scheme is introduced in Section 5. To validate our approach, we present in Section 6 a number of numerical experiments beginning with a simple reference problem of a layered half-space for which experiments with both an axisymmetric 2-D and a full 3-D formulation are performed. We complete the numerical experiments with a series of comparisons with established numerical approaches.

2 THEORETICAL BACKGROUND

The behaviour of the TEM fields after a source current shut-off is described by an initial boundary value problem for Maxwell's equations in quasi-static approximation

$$\nabla \times \boldsymbol{h} - \sigma \boldsymbol{e} = \boldsymbol{j}^e, \tag{1a}$$

$$\partial_t \boldsymbol{b} + \nabla \times \boldsymbol{e} = \boldsymbol{0}, \tag{1b}$$

$$\nabla \cdot \boldsymbol{b} = 0, \tag{1c}$$

where we denote by $\boldsymbol{e}(\boldsymbol{r}, t)$ the electric field, $\boldsymbol{h}(\boldsymbol{r}, t)$ the magnetic field, $\boldsymbol{b}(\boldsymbol{r}, t) = \mu \boldsymbol{h}(\boldsymbol{r}, t)$ the magnetic flux density, $\mu(\boldsymbol{r})$ is the magnetic permeability, and $\boldsymbol{j}^e(\boldsymbol{r}, t)$ external source current density, respectively. The spatial variable $\boldsymbol{r}$ is restricted to a computational domain $\Omega \subset \mathbb{R}^3$ bounded by an artificial boundary Γ, along which appropriate boundary conditions on the tangential components of the fields are imposed, whereas $t \in \mathbb{R}$. The forcing results from a known stationary transmitter source with a driving current which is shut off at time $t = 0$, and hence of the form

$$\boldsymbol{j}^e(\boldsymbol{r}, t) = \boldsymbol{q}(\boldsymbol{r}) H(-t) \tag{2}$$

with the vector field $\boldsymbol{q}$ denoting the spatial current pattern and H the Heaviside step function. The Earth's electrical conductivity is denoted by the parameter $\sigma(\boldsymbol{r})$. We assume negligible coupling between displacement currents and induced magnetic fields, which is valid at late times after current shut-off.

After eliminating $\boldsymbol{b}$ from (1) we obtain the second order partial differential equation

$$\nabla \times (\mu^{-1} \nabla \times \boldsymbol{e}) + \partial_t \sigma \boldsymbol{e} = -\partial_t \boldsymbol{j}^e \quad \text{in } \Omega \tag{3a}$$

for the electric field, which we complete with the perfect conductor boundary condition

$$\boldsymbol{n} \times \boldsymbol{e} = 0 \quad \text{on } \Gamma, \tag{3b}$$

at the outer walls of the model. It should be noted that by doing so, the electric fields at the boundary Γ no longer depend on time t. Switching to the frequency domain, we introduce the Fourier transform pair

$$\boldsymbol{e}(t) = \frac{1}{2\pi} \int_{-\infty}^{\infty} \boldsymbol{E}(\omega)\, e^{i\omega t}\, \mathrm{d}\omega =: (\mathcal{F}^{-1} \boldsymbol{E})(t), \tag{4a}$$

$$\boldsymbol{E}(\omega) = \int_{-\infty}^{\infty} \boldsymbol{e}(t)\, e^{-i\omega t}\, \mathrm{d}t = (\mathcal{F} \boldsymbol{e})(\omega), \tag{4b}$$

ω denoting angular frequency. The representation (4a) can be interpreted as a synthesis of the electric field $\boldsymbol{e}(t)$ from weighted time-harmonic electric partial waves $\boldsymbol{E}(\omega)$, whereas (4b) determines the frequency content of the time-dependent electric field $\boldsymbol{e}$. We thus obtain the transformed version

$$\nabla \times (\mu^{-1} \nabla \times \boldsymbol{E}) + i\omega\sigma \boldsymbol{E} = \boldsymbol{q} \qquad \text{in } \Omega, \tag{5a}$$

$$\boldsymbol{n} \times \boldsymbol{E} = 0 \qquad \text{on } \Gamma, \tag{5b}$$

of (3a) and (3b) provided that solutions exist for all frequencies $\omega \in \mathbb{R}$. In (5a) we have used the fact that, for the time-dependence $e^{i\omega t}$ differentiation with respect to the time variable t becomes multiplication with $i\omega$ in the transformed equations as well as the formal identity $\mathcal{F}[H(-t)] = -1/(i\omega)$, which reflects the fact that the step response due to a current shut-off in a transmitter source is related to an impulsive source by a time derivative $\partial_t H(t) = \delta(t)$, where δ denotes the Dirac impulse, and $\mathcal{F}(\delta) \equiv 1$.

For a given number of discrete frequencies, the Fourier representation (4a) of the solution $\boldsymbol{e}$ of (3) can be utilized to construct an approximate solution in the time domain by a Fourier synthesis. Causality of the field in the time domain allows for a representation of the solution in terms of a sine or cosine transform of the real or imaginary part of $\boldsymbol{e}$, respectively (Newman *et al.* 1986):

$$\boldsymbol{e}(t) = \frac{2}{\pi} \int_0^{\infty} \mathrm{Re}(\boldsymbol{E})\, \frac{\sin \omega t}{\omega}\, \mathrm{d}\omega = \frac{2}{\pi} \int_0^{\infty} \mathrm{Im}(\boldsymbol{E})\, \frac{\cos \omega t}{\omega}\, \mathrm{d}\omega. \tag{6}$$

In practice, the infinite range of integration is restricted to a finite range and the resulting integrals are evaluated by a Fast Hankel Transform (Johansen & Sorensen 1979). For the problems addressed here, solutions for 80–150 frequencies distributed over a broad spectral bandwidth with $f \in [10^{-2}, 10^{9}]$ Hz are required to maintain the desired accuracy.

3 FINITE ELEMENT DISCRETIZATION IN SPACE

For the solution of boundary value problems in geophysics, especially for geo-electromagnetic applications, FD methods have mainly been utilized due to their low implementation effort. However, finite element methods offer many advantages. Using triangular or tetrahedral elements to mesh a computational domain allows for greater flexibility in the parametrization of conductivity structures without the need for staircasing at curved boundaries, such as arise with terrain or seafloor topography. In addition, there is a mature FE convergence theory for electromagnetic applications (Monk 2003). Finally, FE methods are much more suitable for adaptive mesh refinement, adding yet further to their efficiency.

For the construction of a FE approximation, we first express the boundary value problem (5) in variational or weak form (Monk 2003). The weak form requires the equality of both sides of (5a) in the inner product sense only. The $L^2(\Omega)$ inner product of two complex vector fields $\boldsymbol{u}$ and $\boldsymbol{v}$ is defined as

$$(\boldsymbol{u}, \boldsymbol{v}) = \int_{\Omega} \boldsymbol{u} \cdot \bar{\boldsymbol{v}}\, \mathrm{d}V \tag{7}$$

with $\bar{\boldsymbol{v}}$ denoting the complex conjugate of $\boldsymbol{v}$. Taking the inner product of (5a) with a sufficiently smooth (By sufficiently smooth we mean that the mathematical operations that follow are well-defined.) vector field $\boldsymbol{\varphi}$—called the test function—and integrating over Ω, we

Downloaded from https://academic.oup.com/gji/article/173/3/766/736358 by U.S. Department of Justice user on 17 August 2022

obtain after an integration by parts

$$\int_\Omega \left[(\mu^{-1}\nabla\times\boldsymbol{E})\cdot(\nabla\times\bar{\boldsymbol{\varphi}})+i\omega\sigma\boldsymbol{E}\cdot\bar{\boldsymbol{\varphi}}\right]\mathrm{d}V - \int_\Gamma(\boldsymbol{n}\times\bar{\boldsymbol{\varphi}})\cdot(\mu^{-1}\nabla\times\boldsymbol{E})\,\mathrm{d}A=\int_\Omega \boldsymbol{q}\cdot\bar{\boldsymbol{\varphi}}\,\mathrm{d}V. \tag{8}$$

On Γ, the perfect conductor boundary condition (5b) gives no information about $(\mu^{-1}\nabla\times\boldsymbol{E})$, so we eliminate this integral by choosing $\boldsymbol{\varphi}$ such that $\boldsymbol{n}\times\boldsymbol{\varphi}=0$ on Γ, which is the standard way of enforcing the essential boundary condition (5b) in a variational setting.

Introducing the solution space

$$\mathcal{E}:=\{\boldsymbol{v}\in\boldsymbol{H}(\mathrm{curl};\Omega):\boldsymbol{n}\times\boldsymbol{v}=\boldsymbol{0}\text{ on }\Gamma\},$$

in terms of the Sobolev space $\boldsymbol{H}(\mathrm{curl};\Omega)=\left\{\boldsymbol{v}\in L^2(\Omega)^3:\nabla\times\boldsymbol{v}\in L^2(\Omega)^3\right\}$, the weak form of the boundary value problem finally reads

Find $\boldsymbol{E}\in\mathcal{E}$ such that

$$\int_\Omega[(\mu^{-1}\nabla\times\boldsymbol{E})\cdot(\nabla\times\bar{\boldsymbol{v}})+i\omega\sigma\boldsymbol{E}\cdot\bar{\boldsymbol{v}}]\,\mathrm{d}V =\int_\Omega\boldsymbol{q}\cdot\bar{\boldsymbol{v}}\,\mathrm{d}V\qquad\text{for all }\boldsymbol{v}\in\mathcal{E}. \tag{9}$$

Due to the homogeneous boundary condition (5b) the trial and test functions can be chosen from the same space $\mathcal{E}$.

Before describing the FE discretization we note that in the boundary value problem (5) we have already introduced an approximation, namely the perfect conductor boundary condition (5b). This approximation comes about because the boundary Γ of our computational domain Ω is an artificial one in the sense that the physical problem is posed on an infinite domain, and we restrict ourselves to Ω merely for computational convenience. Mathematically, the correct boundary condition on Γ is that resulting in a solution which is the restriction to Ω of the solution on the infinite-domain. Such 'exact' boundary conditions are usually non-local, hence computationally inconvenient, and are often approximated by local boundary conditions such as (5b). The physical justification is, of course, that the electric field decays away from the transmitter source such that, at a sufficient distance, it satisfies (5b) reasonably well. The practical consequence is that Ω must be chosen sufficiently large that the approximation due to the inexact boundary condition posed on Γ is not larger than the discretization error. For high-resolution calculations in 3-D this may result in a large number of unknowns, which is somewhat ameliorated by using adaptively refined meshes. Exact non-local boundary conditions for diffusive geoelectric problems are developed in Goldman *et al.* (1989) and Joly (1989). An overview of exact boundary conditions for problems on truncated domains can be found in Givoli (1992). In the geoelectrics literature this issue is already discussed in the classic paper by Coggon (1971), who in the context of a potential calculation proposes a linear combination of Dirichlet and Neumann boundary conditions along Γ as an effective local boundary condition. Approximate non-local boundary conditions based on integral operators are proposed in the 'hybrid' methods of Gupta *et al.* (1987) and Lee *et al.* (1981) as well as the 'compact FE method' of Gupta *et al.* (1989). Such non-local boundary conditions offer the advantage of allowing computational domains containing only the regions of geophysical interest. In this paper, for simplicity of presentation, we choose to treat this issue by using a sufficiently large computational domain, but note that numerical calculations must take this source of error into account.

To construct a FE solution of the boundary value problem (5) the domain Ω is partitioned into simple geometrical subdomains, for example, triangles for 2-D or tetrahedra for 3-D problems, such that

$$\Omega=\bigcup_{e=1}^{N_e}\Omega_e. \tag{10}$$

The infinite-dimensional function space $\mathcal{E}$ is approximated by a finite dimensional function space $\mathcal{E}^h\subset\mathcal{E}$ of elementwise polynomial functions satisfying the homogeneous boundary condition (5b).

The approximate electric field $\boldsymbol{E}^h\approx\boldsymbol{E}$ is defined as the solution of the discrete variational problem obtained by replacing $\mathcal{E}$ by $\mathcal{E}^h$ in (9) (*cf.* Monk 2003).

To obtain the matrix form of (9), we express $\boldsymbol{E}^h$ as a linear combination of basis functions $\{\boldsymbol{\varphi}_i\}_{i=1}^N$ of $\mathcal{E}^h$, that is,

$$\boldsymbol{E}(\boldsymbol{r})=\sum_{i=1}^N E_i\,\boldsymbol{\varphi}_i(\boldsymbol{r}). \tag{11}$$

Testing against all functions in $\mathcal{E}^h$ is equivalent to testing against all basis functions $\boldsymbol{\varphi}_j$, $j=1,\ldots,N$. Taking the jth basis function as the test function and inserting (11) into (9) yields the jth row of a linear system of equations

$$(\mathbf{K}+i\omega\mathbf{M})\,\mathbf{u}=\mathbf{f} \tag{12}$$

for the unknown coefficients $E_i=[\mathbf{u}]_i$, $i=1,\ldots,N$, where

$$[\mathbf{K}]_{j,i}=\int_\Omega(\mu^{-1}\nabla\times\boldsymbol{\varphi}_i)\cdot(\nabla\times\bar{\boldsymbol{\varphi}}_j)\,\mathrm{d}V, \tag{13}$$

$$[\mathbf{M}]_{j,i}=\int_\Omega\sigma\boldsymbol{\varphi}_i\cdot\bar{\boldsymbol{\varphi}}_j\,\mathrm{d}V, \tag{14}$$

$$[\mathbf{f}]_j=\int_\Omega\boldsymbol{q}\cdot\bar{\boldsymbol{\varphi}}_j\,\mathrm{d}V. \tag{15}$$

The matrices $\mathbf{K}$ and $\mathbf{M}$, known as 'stiffness' and 'mass matrix', respectively, in FE parlance, are large and sparse and, since μ and σ are real-valued quantities in the problem under consideration, consist of real entries.

For a given source vector $\mathbf{f}$ determined by the right-hand side of (5a), the solution vector $\mathbf{u}\in\mathbb{C}^N$ of (12) yields the approximation $\boldsymbol{E}^h$ of the electric field $\boldsymbol{E}$ we wish to determine.

4 MODEL REDUCTION

Our goal is the efficient computation of the FE approximation $\boldsymbol{E}^h$ in a subset of the computational domain Ω. To this end, we fix a subset of $p\ll N$ components of the solution vector $\mathbf{u}$ to be computed. These correspond to p coefficients in the FE basis expansion (11), and thus, in the lowest-order Nédélec spaces we have employed, directly to components of the approximate electric field $\boldsymbol{E}^h$ along selected edges of the mesh. We introduce the discrete extension operator $\mathbf{E}\in\mathbb{R}^{N\times p}$ defined as

$$[\mathbf{E}_{i,j}]=\begin{cases}1, & \text{if the } j\text{th coefficient to be computed}\\ & \text{has global index } i,\\ 0, & \text{otherwise.}\end{cases}$$

Multiplication of a coefficient vector $\mathbf{v}\in\mathbb{C}^N$ with respect to the FE basis by $\mathbf{E}^\top$ then extracts the p desired components, yielding the reduced vector $\mathbf{E}^\top\mathbf{v}\in\mathbb{C}^p$ containing the field values at the points of interest.

For the solution $\mathbf{u}$, this reduced vector, as a function of frequency, thus takes the form

$$\mathbf{t}=\mathbf{t}(\omega)=\mathbf{E}^\top(\mathbf{K}+i\omega\mathbf{M})^{-1}\mathbf{f}\in\mathbb{C}^p. \tag{16}$$

© 2008 The Authors, *GJI*, **173,** 766–780
Journal compilation © 2008 RAS

Downloaded from https://academic.oup.com/gji/article/173/3/766/736358 by U.S. Department of Justice user on 17 August 2022

The vector-valued function $\mathbf{t}(\omega)$ in eq. (16) assigns, to each frequency ω, the output values of interest to the source (input) data represented by the right-hand-side vector $\mathbf{f}$.

Computing $\mathbf{t}(\omega)$ for a given number of frequencies $\omega_j \in [\omega_{\min}, \omega_{\max}]$, $j = 1, \ldots, N_f$, by solving N_f full systems and then extracting the p desired components from each is computationally expensive, if not prohibitive, for large N. This situation is similar to that of linear systems theory, where the function $\mathbf{t}$ is known as a 'transfer function' and the objective is to approximate $\mathbf{t}$ based on a model with significantly fewer degrees of freedom than N, hence the term 'model reduction'.

To employ model reduction techniques, we proceed by fixing a reference frequency ω_0 and rewriting (16) as

$$\mathbf{t} = \mathbf{t}(s) = \mathbf{E}^\top [\mathbf{A}_0 - s\mathbf{M}]^{-1}\mathbf{f}, \qquad \mathbf{A}_0 := \mathbf{K} + i\omega_0\mathbf{M}, \tag{17}$$

where we have also introduced the (purely imaginary) 'shift parameter' $s = s(\omega) := i(\omega_0 - \omega)$. Setting further $\mathbf{L} := \mathbf{E} \in \mathbb{R}^{N\times p}$, $\mathbf{r} := \mathbf{A}_0^{-1}\mathbf{f} \in \mathbb{C}^N$, and $\mathbf{A} := \mathbf{A}_0^{-1}\mathbf{M} \in \mathbb{C}^{N\times N}$, the transfer function becomes

$$\mathbf{t}(s) = \mathbf{L}^\top (\mathbf{I} - s\mathbf{A})^{-1}\mathbf{r}. \tag{18}$$

The transfer function is a rational function of s (and hence of ω), and a large class of model reduction methods consist of finding lower order rational approximations to $\mathbf{t}(s)$. The method we propose constructs a Padé-type approximation with respect to the expansion point ω_0, that is, $s = 0$. The standard approach (Gragg & Lindquis 1983; Freund 2003; Antoulas 2005) for computing such approximations in a numerically stable way is by Krylov subspace projection. For simplicity, we consider an orthogonal projection onto a Krylov space based on Arnoldi's method.

For an arbitrary square matrix $\mathbf{C}$ and non-zero initial vector $\mathbf{x}$, the Arnoldi process successively generates orthonormal basis vectors of the nested sequence

$$\mathcal{K}_m(\mathbf{C}, \mathbf{x}) := \operatorname{span}\{\mathbf{x}, \mathbf{C}\mathbf{x}, \ldots, \mathbf{C}^{m-1}\mathbf{x}\}, \qquad m = 1, 2, \ldots$$

of 'Krylov spaces' generated by $\mathbf{C}$ and $\mathbf{x}$, which are subspaces of dimension m up until m reaches a unique index L, called the grade of $\mathbf{C}$ with respect to $\mathbf{x}$, after which these spaces become stationary. In particular, choosing $\mathbf{C} = \mathbf{A}$ and $\mathbf{x} = \mathbf{r}$, m steps of the Arnoldi process result in the 'Arnoldi decomposition'

$$\mathbf{A}\mathbf{V}_m = \mathbf{V}_m\mathbf{H}_m + \eta_{m+1,m}\mathbf{v}_{m+1}\mathbf{e}_m^\top, \qquad \mathbf{r} = \beta\mathbf{v}_1, \tag{19}$$

in which the columns of $\mathbf{V}_m \in \mathbb{C}^{N\times m}$ form an orthonormal basis of $\mathcal{K}_m(\mathbf{A}, \mathbf{r})$, $\mathbf{H}_m \in \mathbb{C}^{m\times m}$ is an unreduced upper Hessenberg matrix, $\mathbf{v}_{m+1}$ is a unit vector orthogonal to $\mathcal{K}_m(\mathbf{A}, \mathbf{r})$ and $\mathbf{e}_m$ denotes the mth unit coordinate vector in $\mathbb{C}^m$. In particular, we have the relation $\mathbf{H}_m = \mathbf{V}_m^\top\mathbf{A}\mathbf{V}_m$. Using the orthonormal basis $\mathbf{V}_m$, we may project the vector $\mathbf{r}$ as well as the columns of $\mathbf{L}$ in (18) orthogonally onto $\mathcal{K}_m(\mathbf{A}, \mathbf{r})$ and replace the matrix $\mathbf{I} - s\mathbf{A}$ by its compression $\mathbf{V}_m^\top(\mathbf{I} - s\mathbf{A})\mathbf{V}_m$ onto $\mathcal{K}_m(\mathbf{A}, \mathbf{r})$. This yields the approximate transfer function

$$\begin{aligned}\mathbf{t}_m(s) &:= \left(\mathbf{V}_m^\top\mathbf{L}\right)^\top \left[\mathbf{V}_m^\top\left(\mathbf{I} - s\mathbf{A}\right)\mathbf{V}_m\right]^{-1}\left(\mathbf{V}_m^\top\mathbf{r}\right) \\ &= \mathbf{L}_m^\top(\mathbf{I}_m - s\mathbf{H}_m)^{-1}\beta\mathbf{e}_1,\end{aligned} \tag{20}$$

where we have set $\mathbf{L}_m := \mathbf{V}_m^\top\mathbf{L}$ and used the properties of the quantities in the Arnoldi decomposition (19).

Given the task of evaluating the transfer function (16) for N_f frequencies $\omega_j \in [\omega_{\min}, \omega_{\max}]$, our model reduction approach, to which we refer as 'model reduction in the frequency domain' (MRFD), now proceeds as detailed in Algorithm 1.

Algorithm 1 Model reduction for TEM in the frequency domain (MRFD).

FE discretization of problem (5) yields matrices $\mathbf{K}$ and $\mathbf{M}$.
Select a reference frequency $\omega_0 \in [\omega_{\min}, \omega_{\max}]$.
Set $\mathbf{A}_0 := \mathbf{K} + i\omega_0\mathbf{M}$, $\mathbf{A} := \mathbf{A}_0^{-1}\mathbf{M}$ and $\mathbf{r} := \mathbf{A}_0^{-1}\mathbf{f}$.
Perform m steps of the Arnoldi process applied to $\mathbf{A}$ and $\mathbf{r}$ yielding decomposition (19).
for $j = 1, 2, \ldots, N_f$ **do**
  Set $s_j := \omega_0 - \omega_j$
  Evaluate approximate transfer function $\mathbf{t}_m(s_j)$
  according to (20).;

Note that computations with large system matrices and vectors with the full number N of degrees of freedom are required only in the Arnoldi process, after which the loop across the target frequencies takes place in a subspace of much smaller dimension $m \ll N$. As a consequence, the work required in the latter is almost negligible in comparison. Within the Arnoldi process the most expensive step is the matrix-vector multiplication with the matrix $\mathbf{A} = \mathbf{A}_0^{-1}\mathbf{M}$. Currently, we compute an LU factorization of $\mathbf{A}_0$ in a pre-processing step and use the factors to compute the product with two triangular solves.

We note that it may be more efficient to use more than one reference frequency to cover the frequency band of interest. In this case, one may either use separate Krylov subspaces for the different parts of the interval $[\omega_{\min}, \omega_{\max}]$, necessitating additional LU factorizations. Alternatively, one could use one subspace consisting of the sum of the Krylov spaces associated with each reference frequency. In Section 6, we give such an example using the former approach in which two reference frequencies lead to sufficient approximations in less computer time than if only one is used. Current Krylov subspace-based model reduction techniques in other disciplines employ much more refined subspace generation techniques, in particular block algorithms to take into account all columns of $\mathbf{L}$ in the subspace generation as well as two-sided Lanczos (Feldmann & Freund 1994) and Arnoldi (Antoulas 2005) methods to increase the approximation order of the transfer function. We intend to explore these refinements for the present TEM application in future work. However, we have been able to obtain surprisingly good results using this very basic method. A further enhancement is replacing the LU factorization of $\mathbf{A}_0$ with an inner iteration once the former is no longer feasible due to memory constraints.

For the simple model reduction approach taken here involving only a Krylov subspace generated by $\mathbf{A}$ and the 'right' vector $\mathbf{r}$ in (18), an error analysis of our MRFD method may be carried out using the theory of matrix functions (*cf.* Saad 1992) to arrive at an asymptotic convergence rate of the MRFD approximation with respect to m depending on spectral properties of $\mathbf{K}$ and $\mathbf{M}$. Such an analysis is beyond the scope of this article and will be published elsewhere.

5 NUMERICAL EXPERIMENTS

To validate the MFRD method we present a number of numerical experiments. We begin with the very simple reference problem of a vertical magnetic dipole source over a layered half-space, and perform a number of experiments with both a 2-D axisymmetric and a full 3-D formulation. The reason for including this somewhat academic example is that an analytic solution is available for comparison against the numerical approximation, thus permitting an easy calibration of the size of the computational domain

Downloaded from https://academic.oup.com/gji/article/173/3/766/736358 by U.S. Department of Justice user on 17 August 2022

(the distance of the outer boundary) as well as the mesh resolution required to ensure the dominant error is due to the Krylov subspace projection. We discuss the behaviour of the MRFD approximation with respect to the size of the Krylov space as well as the location and number of reference frequencies. We conclude with a series of comparisons of our method with established approaches such as SLDM and explicit FDTD on more realistic and challenging 3-D conductivity structures.

In all experiments the FE discretization was carried out using the Electromagnetics Module of the COMSOL Multiphysics package, where we have used second order Lagrange elements on triangles in the 2-D calculations and second order elements from Nédélec's first family on tetrahedra for 3-D.

The sparse LU decomposition required in our algorithm as well as the triangular solves based on this decomposition were performed using the PARDISO software of Schenk & Gärtner (2004, 2006). Our own code is written in MATLAB, from where the appropriate COMSOL and PARDISO components are called. All computations were carried out on a 3.0 GHz Intel Xeon 5160 with 16 GB RAM running Suse Linux 10.1.

In the discussions of the numerical experiments we specify frequencies in Hertz denoted by $f = \omega/(2\pi)$.

5.1 The layered half-space

We begin with a layered half-space conductivity structure depicted in Fig. 1 consisting of a 30 Ω m layer of thickness 30 m at a depth of 100 m which is embedded in a uniform half-space of 100 Ω m. The source is a vertical magnetic dipole at the surface $z = 0$. For the analytical reference solution we employ the quasi-static approximation of Ward & Hohmann (1988), from which we obtain the time-domain solution via a Hankel transform. The numerical results obtained by the MRFD method are compared with the analytical 1-D model results for the approximate electric field obtained from the transfer function $\mathbf{t}_m$ as well as the transient electric field obtained by Fourier synthesis of the transfer function.

The discrete set of frequencies at which a solution is sought is given by $f_i \in [10^{-2}, 10^9]$ Hz with 10 logarithmically equidistant frequencies per decade, giving a total of 110 target frequencies. This range of frequencies corresponds to a time interval of $[10^{-6}, 10^{-3}]$s for the evaluation of the transient.

Each mesh that we use for the spatial discretization is refined in the vicinity of the source to capture its singular behaviour. The refinements result from three successive adaptive mesh refinement steps of COMSOL's default *a posteriori* error estimator, in which the mesh refinement is performed by remeshing.

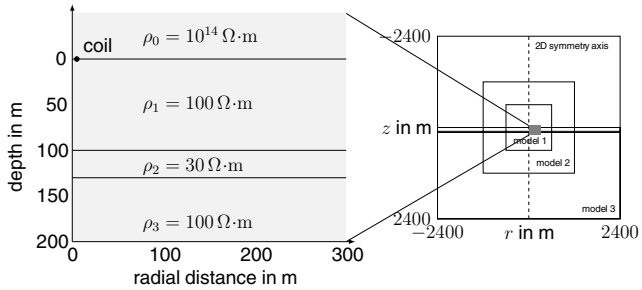

Figure 1. Cross-section of the layered half-space conductivity model. The conductive layer is 30 m thick. The dimension of the discretized models 1, 2 and 3 extends to up to ± 600, ±1200 and ±2400 m in the horizontal and vertical directions. In the 2-D formulation the axis of symmetry is aligned with the z-axis.

5.1.1 2-D axisymmetric formulation

In the 2-D axisymmetric configuration the dipole source is aligned with the z-axis of a cylindrical coordinate system and approximated by a finite circular coil of radius 5 m. The electric field is thus aligned with the azimuthal direction and we obtain a scalar problem for this component. The computational domain Ω is the rectangle $\{(r, z) : 0 \le r \le r_{\max}, -z_{\max} \le z \le z_{\max}\}$ in the vertical r–z plane. Fig. 2 shows the three computational domains we consider, corresponding to the values $r_{\max} = z_{\max} = 600$, 1200 and 2400 m, respectively. The source coil is modelled as a point source located at $r_0 = 5$, $z_0 = 0$, and we consider the fixed evaluation point $r_1 = 100$, $z_1 = 0$ located on the surface at a distance of 100 m from the dipole source. The mesh generation is carried out in such a way that (r_1, z_1) is a triangle vertex, and therefore, the value of the FE approximation there corresponds exactly to a degree of freedom. With $I = 1/(\pi r_0^2)$ A denoting the current in the coil, chosen to result in a unit dipole moment, and Γ_0 denoting the portion of the domain boundary on the symmetry axis $r = 0$, the 2-D axisymmetric formulation of the boundary value problem (5) reads

$$-\partial_r\left[\frac{1}{\mu r}\partial_r(rE_\phi)\right] - \partial_z\left(\mu^{-1}\partial_z E_\phi\right) + i\omega\sigma E_\phi, \\ = i\omega I\delta(r - r_0)\delta(z - z_0) \quad \text{in } \Omega, \tag{21a}$$

$$E_\phi = 0 \quad \text{on } \Gamma \setminus \Gamma_0, \tag{21b}$$

$$\partial_r E_\phi = 0 \quad \text{on } \Gamma_0. \tag{21c}$$

The FE discretization uses second-order (node-based) Lagrange elements on a triangular mesh and Fig. 2 also shows a triangular mesh for each domain with 5254, 8004 and 13 417 degrees of freedom, respectively.

We begin by illustrating the effects of the mesh width and the location of the outer boundary Γ. To this end we consider the three domains and meshes shown in Fig. 2. The meshes were chosen to yield comparable resolution for each domain, with a refinement near the magnetic dipole source and in the high-conductivity layer.

The FE discretization contains two sources of error: one arising from the usual dependence of the error on the mesh width, that is, resolution, the other arising from imposing the physically non-exact boundary condition (21b) or (5b), respectively, at the non-symmetry boundaries. As we are modelling a diffusion process, the error due to the boundary condition decreases rapidly with the size of the computational domain. An efficient discretization should balance these two types of error, that is, the domain size and mesh width should be chosen such that these two errors are of comparable magnitude. Since, for each frequency ω, we are solving a damped wave equation in which damping increases with frequency (at fixed conductivity), the solutions at higher frequencies decay faster towards the outer boundary. Therefore, the effect of the error due to the non-exact boundary condition is greatest at the lowest frequency. In the time domain this corresponds to late times, when all but the low frequency components have decayed. The mesh resolution, on the other hand, will result in the largest error at the highest frequency. This error, however, is less problematic due to the $1/\omega$ factor in the Hankel transform (6) which damps the high-frequency errors.

In order to clearly distinguish the errors resulting from the discretization parameters mesh resolution and boundary placement from those associated with the Krylov subspace projection, we first carry out a naive 'brute-force' frequency-domain calculation in which we solve the full problem (12) for each frequency. The upper left-hand plot in Fig. 3 shows the real part of the transfer

Downloaded from https://academic.oup.com/gji/article/173/3/766/736358 by U.S. Department of Justice user on 17 August 2022

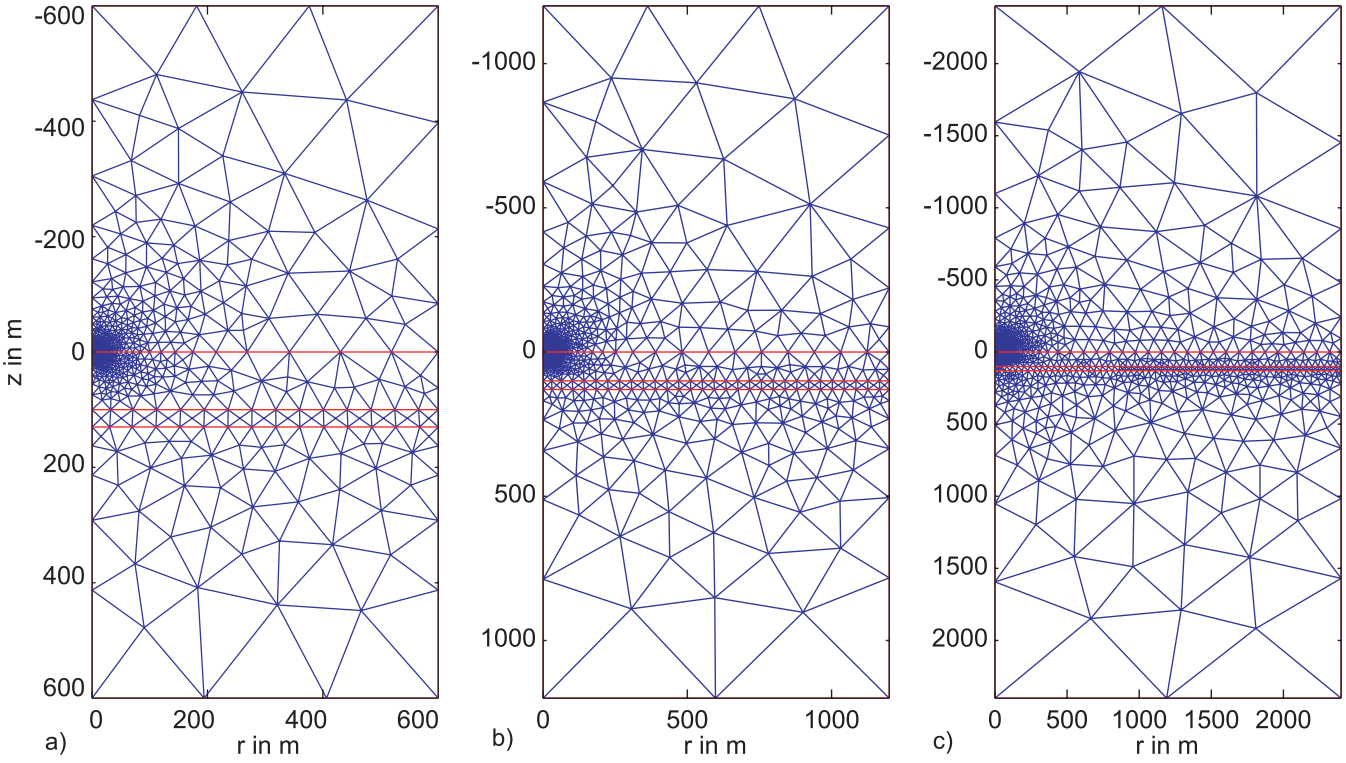

Figure 2. Finite element meshes for the 2-D formulation (from left- to right-hand side) for model 1 (5254 DOFS, width 600 m), model 2 (8004 DOFS, width 1200 m), and model 3 (13 417 DOFS, width 2400 m).

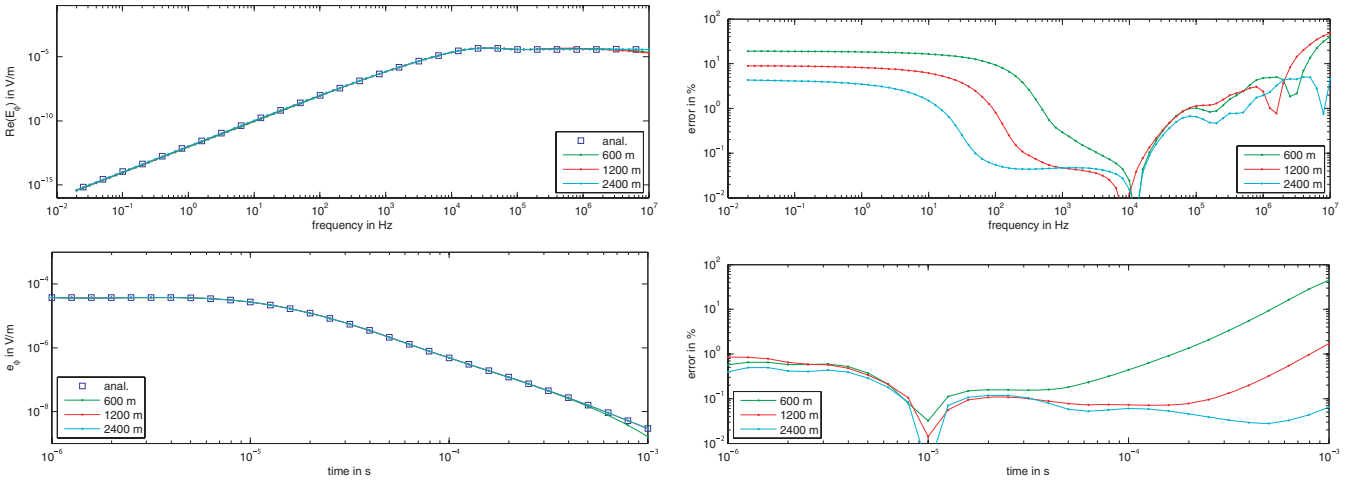

Figure 3. Real part of transfer function **t** computed by direct evaluation of (12) (upper left-hand side), transient $e_\phi(t)$ (lower left-hand side), and associated relative errors (right-hand column) for different domain sizes.

function Re $E_\phi(f)$ obtained this way evaluated at the receiver point (r_1, z_1). We observe good agreement with the analytical solution for all three domains. Looking at the error in the transfer function in the upper right-hand plot reveals the effect of the error due to the boundary condition in the low frequencies, which is seen to decrease as the domain is enlarged. At the high frequencies the somewhat finer resolution used for the largest domain results in the smallest error here. The synthesized transient is displayed on the lower left-hand side, showing excellent agreement for all domain sizes with the two smaller domains displaying a slightly larger error for late times due to the larger low-frequency error. This observation is more pronounced in the plot on the lower right-hand side showing the error in the transient. The early-time errors, in particular, show that the mesh resolution is sufficient in all three cases.

Fig. 4 displays the result of solving the problem on the 1200 m domain using the MRFD algorithm with a single reference frequency $f_0 = 10^3$ Hz and a Krylov subspace of dimension $m = 20$, 50, 100 and 200, respectively. In the transfer function plot on the upper left-hand side and the corresponding error plot on the upper right, we observe good agreement with the analytic solution for all values of m up until a frequency of $f = 10^5$ Hz at which point the approxi-

Downloaded from https://academic.oup.com/gji/article/173/3/766/736358 by U.S. Department of Justice user on 17 August 2022

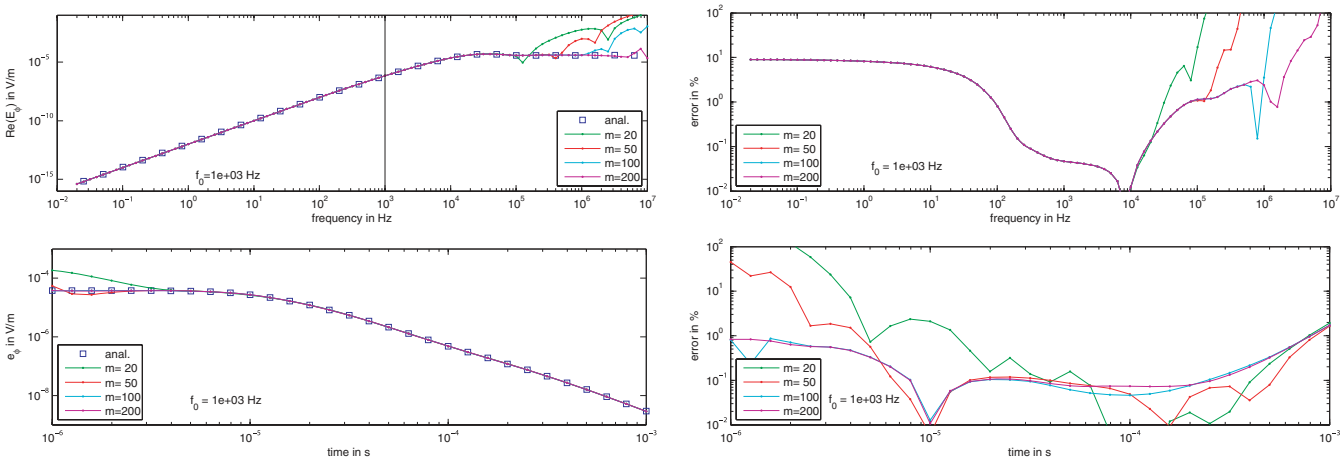

Figure 4. Real part of transfer function $\mathbf{t}_m$ (upper left-hand side), transient $e_\phi(t)$ (lower left-hand side), and associated relative error (right-hand column) computed for $f_0 = 10^3$ Hz. 2-D model size 1 200 m.

mation with $m = 20$ begins to deteriorate. When the dimension $m = 200$ is reached we observe a sufficient approximation across all frequencies. In the transients, however, we note that the high-frequency errors for all approximations have been damped, and it is the error for frequencies greater than 10^5 Hz that makes the $m = 20$ and 50 approximations inaccurate at early times.

To give an indication of the gain in efficiency from using the MRFD approach we note that, for the 1200 m domain with 8004 degrees of freedom, the total computing time necessary to reach convergence with a Krylov subspace dimension of $m = 100$ was 6.1 s, compared with 21 s for the brute-force variant of evaluating eq. (12) directly for same 110 frequencies. We note, however, that this gain in speed becomes much more pronounced for large scale 3-D problems where a direct computation of the transfer function is not advisable.

In Fig. 5, we illustrate the dependence of the MRFD approximation on the choice of the reference frequency f_0 for the 1200 m domain by comparing the results for the five reference frequencies $f_0 = 0, 10^2, 10^4, 10^5$ and 10^6 Hz, respectively. Fig. 5(a) shows the result for $f_0 = 0$ Hz, which corresponds to the SLDM variant proposed in Druskin *et al.* (1999). We observe good agreement with the analytical solution for the low-frequency part independent of the Krylov space dimension, whereas for the higher frequencies with $f > 10^5$ Hz the approximate transfer function deteriorates even for the largest considered Krylov subspace of dimension $m = 200$. This observation corresponds to a substantial error in the transient for early times, which likewise decreases with increasing Krylov space dimension. With increasing reference frequency f_0 (*cf.* Figs 5b–e), the part of the transfer function which agrees well with the analytical solution gets shifted towards higher frequencies until, for $f_0 = 10^6$ Hz, a reasonable fit can be established even with the small Krylov space of dimension $m = 20$. Moreover, the deficiency in the low frequency part of the transfer function causes considerable error in the late time part of the transient, which is not eliminated up to $m = 200$. A sufficiently good approximation of the transient at late times would thus require a much larger Krylov space for this reference frequency.

5.1.2 3-D formulation

In the 3-D formulation we discretize the full electric field using second-order tetrahedral Nédélec (vector) elements on a cube of edge length 2400 m centred at the origin. The degrees of freedom of the FE approximation are, therefore, associated with the edges and faces of the tetrahedral elements. The vertical magnetic dipole source is approximated by a square loop of 10 m edge length located in the plane defined by $z = 0$ centred at the origin. Electric currents flowing inside the loop are associated with currents assigned to the edges of those tetrahedral elements which coincide with the loop position. The receiver, centred at the point $(x = 100, y = 0, z = 0)$ m, that is, 100 m away from the centre of the coplanar transmitter loop, is formed by a square loop of 4 m edge length. The y-components of the electric fields in the receiver loop are thus associated with the two edges perpendicular to the x-direction at $x = 98$ and 102 m, respectively. Analogously, the x-components of the electric field can be obtained at $y = -2$ and 2 m and $x = 100$ m. Fig. 6 shows a horizontal cross-section of the 3-D tetrahedral mesh at $z = 0$, displaying the distribution of the tetrahedra refined near the source as in the 2-D case. The complete 3-D mesh consists of 12 218 tetrahedra, which corresponds to 79 844 degrees of freedom. We note that second-order tetrahedral elements of Nédélec's first family have 20 degrees of freedom per element and that the number of global degrees of freedom scale roughly as 6 times the number of tetrahedra. Again, the mesh is generated in such a way that the four segments of the receiver coil coincide with edges of tetrahedra. In evaluating the transfer function, we determine the electric field along one of these four edges, namely that centred at $(x = 98, y = 0, z = 0)$ m and oriented in the y-direction, which again corresponds to one FE degree of freedom.

Figs 7(a)–(c) shows the real part of the approximated transfer function $\mathbf{t}_m$ for the 3-D discretization for the Krylov subspace dimensions $m = 20$, 50 and 200 and reference frequencies $f_0 = 10^2$, 10^3, 10^4 and 10^5 Hz.

As in the 2-D case (*cf.* Fig. 5), the error between analytical and approximate transfer function is small near the reference frequency, whereas the deviation in the low frequency part is larger than in the 2-D case. For $f_0 = 10^2$ Hz the relative error of the transient (Fig. 7a, right-hand side) is large for early times. Adding more Krylov vectors does not improve the agreement. However, increasing the Krylov dimension improves the agreement at late times significantly. The latter is bounded by a lower limit imposed by the distance of the domain boundaries, a discretization feature which cannot be compensated by a larger Krylov space, but can only be further reduced by a larger computational domain. By increasing the reference

© 2008 The Authors, *GJI*, **173,** 766–780
Journal compilation © 2008 RAS

Downloaded from https://academic.oup.com/gji/article/173/3/766/736358 by U.S. Department of Justice user on 17 August 2022

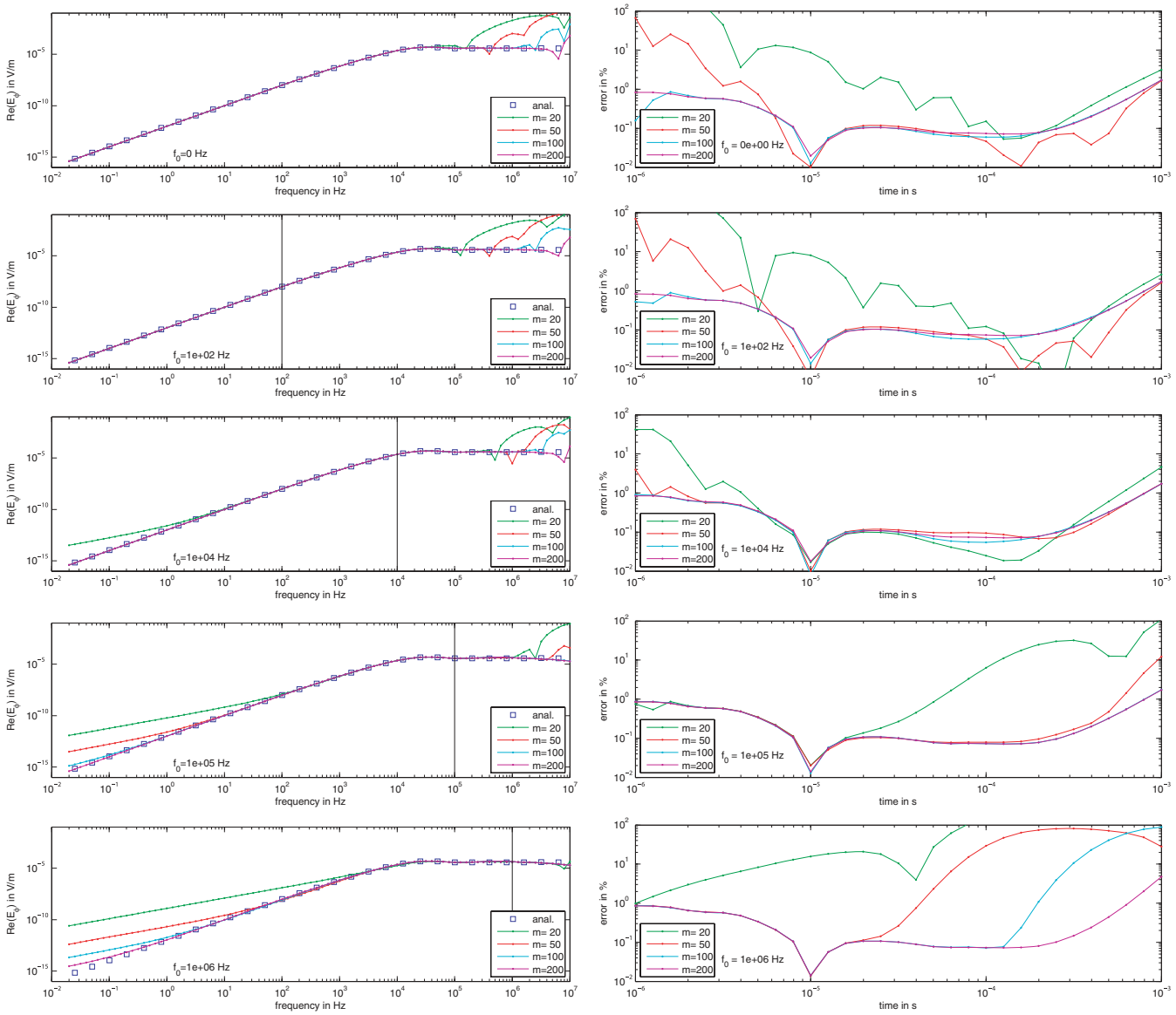

Figure 5. Real part of transfer function $\mathbf{t}_m$ (left-hand side) and associated relative error of transient electric field (right-hand side) for different Krylov subspace dimensions and reference frequencies. 2-D model size 1200 m.

frequency (*cf.* Figs 7b–c), the error in the early times can be further reduced. Attaining better agreement at late times would require a larger Krylov space.

Again as in the 2-D example, we observe that the Hankel transform in the synthesis of the time domain solution effectively damps out the errors in the transfer function in the high frequencies $f > 10^6$ Hz, resulting in good agreement of the transient with the analytical solution for a Krylov subspace dimension of $m = 200$. Closer inspection of the approximate transfer functions for different reference frequencies indicates that 'local' convergence near the reference frequencies is observable already for small Krylov subspace dimensions. Therefore, it seems attractive to construct an improved approximation of the transfer function by incorporating more than one reference frequency into the MRFD process.

The benefit of using approximate transfer functions associated with several reference frequencies and separate, low-dimensional Krylov spaces is twofold: first, the accuracy may be enhanced significantly, particularly at late times of the transient. On the other hand, smaller Krylov spaces results in a significant decrease of the computational effort.

Fig. 8 shows the gain in accuracy when using two reference frequencies. Using 40 Krylov subspace basis vectors for $f_0 = 10^2$ Hz and 100 Krylov subspace basis vectors for $f_0 = 10^4$ Hz, the fit of the approximated transfer function $\mathbf{t}_m$ is good for a frequency band from 10 to 10^6 Hz. The transient electric field at the receiver shows an equally good agreement for both early and late times. The relative error between approximate and analytical transient is less than 1.5 per cent over the complete time interval.

The computational cost of the MRFD method is dominated by the LU factorization of the matrix $\mathbf{A}_0$ as well as the triangular backsolves based on this factorization at each step of the Arnoldi process. Fig. 9 gives a breakdown of the computer time required for the MRFD algorithm applied the 3-D layered half-space model using one and two reference frequencies. For the model with 79 844 degrees of freedom one LU factorization requires 12 s of computing time. Once an LU factorization is available the Krylov subspace is

Downloaded from https://academic.oup.com/gji/article/173/3/766/736358 by U.S. Department of Justice user on 17 August 2022

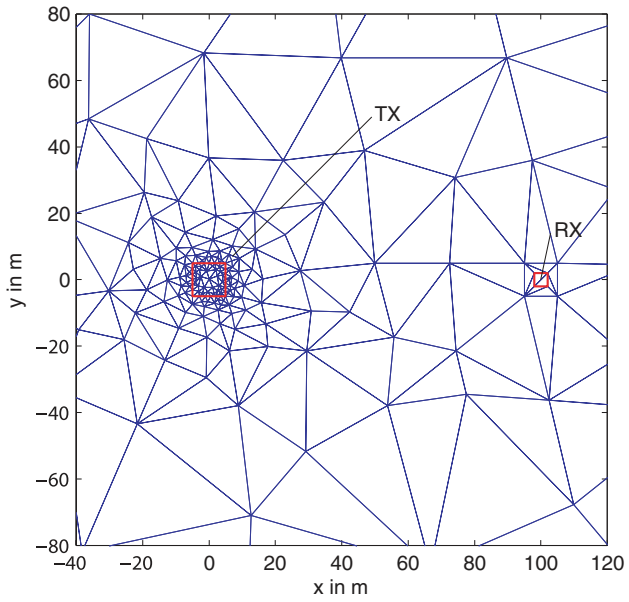

Figure 6. Horizontal cross-section of the 3-D finite element mesh (plane at $z = 0$) used for numerical experiments. A total of 500 triangular boundary faces are aligned with the interface at $z = 0$. The full 3-D mesh consists of 12 218 tetrahedral elements corresponding to 79 844 DOFS. Transmitter and receiver loops are denoted by TX and RX, respectively.

constructed requiring only triangular backsolves utilizing the LU factors. The computational effort grows quadratically with the Krylov space dimension. Hence, the total computing time for the MRFD method is dominated by the construction of a sufficiently large Krylov subspace. The final step of Fourier transforming the approximate transfer function into the time domain adds only negligible effort.

When only one reference frequency is used the total CPU time for the MRFD method is 280 s, including 12 s for one LU factorization, 267.28 s for construction of 200 Krylov basis vectors, and remaining 0.72 s for transforming the transfer function into the time domain. Therefore, once the Arnoldi basis of the Krylov space has been generated, the cost of the sweep over the remaining frequencies is essentially negligible in comparison to that of the Arnoldi process.

Since each new reference frequency requires the LU factorization of a new matrix $\mathbf{A}_0$, we require as many LU factorizations as reference frequencies. Our numerical experiments have shown that, due to the limited complexity of the layered half-space model two reference frequencies are sufficient.

In this case the time required for the two LU factorizations is 24 s. Building up the low frequency part of the transfer function associated with the Krylov basis for $f_0 = 10^2$ Hz requires 40 Arnoldi steps and 25.5 s. The second reference frequency is associated with the build-up of the high frequency part of the transfer function. The construction of its Krylov basis with $m = 100$ takes 89.5 s. The total computing time amounts 138.5 s including 0.35 s required for the concluding Hankel transform. Incorporating yet further reference frequencies will save further computer time as long as the savings in the Krylov part compensate the increased effort of the additional LU factorizations.

5.2 Agreement with other numerical approaches

We further compare the accuracy of the MRFD method against results obtained by the SLDM (Druskin & Knizhnerman 1988) and the FDTD method (Commer & Newman 2004). To this end, more complex, non-trivial conductivity models relevant to geo-electromagnetic applications in ore and marine exploration will be considered.

5.2.1 *Layered half-space model*

The first example compares the layered half-space model response with an SLDM solution. The FD grid used with the SLDM experiment is depicted in Fig. 10. Due to the nature of the tensor product grids used there, unnecessarily fine grid cells occur at the outer boundaries of the discretized region.

Both meshes lead to solutions of comparable accuracy. However, compared with a solution vector of 108 000 entries for the SLDM approach, the total number of degrees of freedom is only 79 844 for the adaptively refined FE discretization (*cf.* Fig. 6).

Fig. 11 shows a comparison of the transient electric field at $x = 98$ m computed with our MRFD approach with that produced by the SLDM method. We observe excellent agreement of both approximations.

5.2.2 *Complex conductivity model*

Next, we consider a conductivity model with a complex 3-D conductor at a vertical contact presented by Commer & Newman (2004). The model section in Fig. 12 consists of a 1 Ω m dipping body at a vertical contact of two resistors of 100 and 300 Ω m covered by a thin 10 Ω m conductive layer. The transmitter source is an electric line source of 100 m length layered out perpendicular to the profile, parallel to the strike of the conductor.

The computational domain for the 3-D FE model is a box of 4 000 m side length. The entire mesh consists of 34 295 tetrahedra, which corresponds to 214 274 degrees of freedom. The considered time interval of the transient suggested the choice of two reference frequencies with $f_0 = 10$ and 10^2 Hz. For both frequencies, the desired dimension of the Krylov subspace has been chosen to be $m = 40$.

Fig. 13 shows the transient electric field measured perpendicular to the profile at three different locations on a profile in comparison with results obtained with the FDTD method. In general, the solutions compare well for all receiver positions especially at early times. The largest deviation occures at late times for the receiver 900 m away from the transmitter. We note however, that the time of the sign reversals fit very well.

5.2.3 *Marine EM simulation*

We conclude our numerical experiments with a model situation which is typical for the emerging sector of marine controlled source electromagnetic applications (Edwards 2005). An electric dipole source will be used as a transmitter which is laid out at the seafloor. A set of receivers measure the inline electric field components after source current turn-off (Fig. 14).

As a numerical example, we consider the case of a small resistive body embedded in a good conducting environment. The computational domain is a box of 2400 m side length. The mesh consists of 12 147 tetrahedral elements corresponding to 76 388 degrees of freedom. As reference frequencies, 10^2 and 10^4 Hz have been choosen with a desired Krylov subspace dimension of $m = 50$ for both cases. The source is an electric dipole which is laid out at the seafloor in profile direction. Measurements of the in-line electric fields are taken

Downloaded from https://academic.oup.com/gji/article/173/3/766/736358 by U.S. Department of Justice user on 17 August 2022

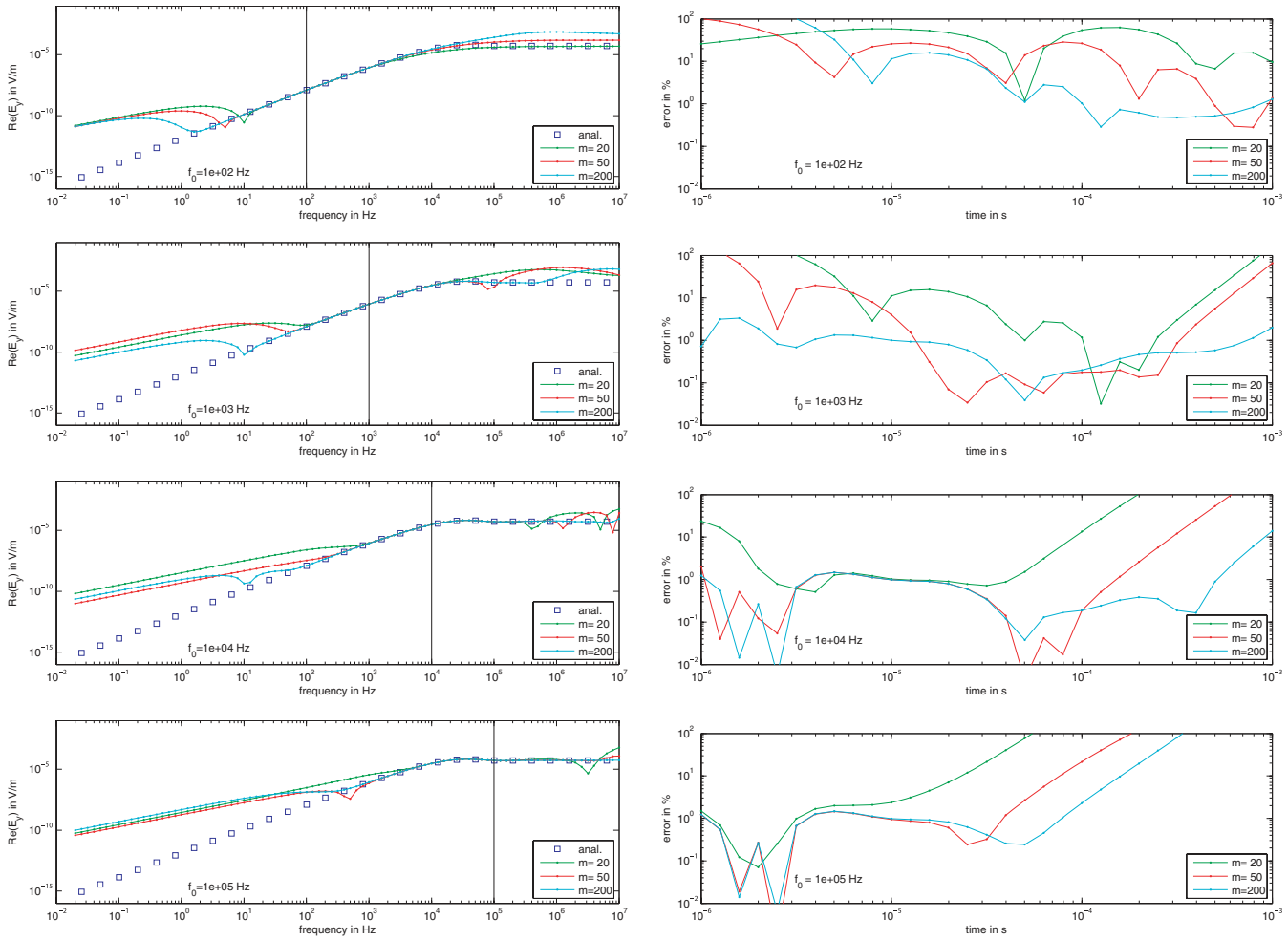

Figure 7. Real part of transfer function $\mathbf{t}_m$ (left-hand side) and associated relative error of transient (right-hand side) at $x = 98$ m for different Krylov subspace dimensions, reference frequency $f_0 = 10^2$ Hz (a), $f_0 = 10^3$ Hz (b), $f_0 = 10^4$ Hz (c), $f_0 = 10^5$ Hz (d), 3-D model size 2400 m.

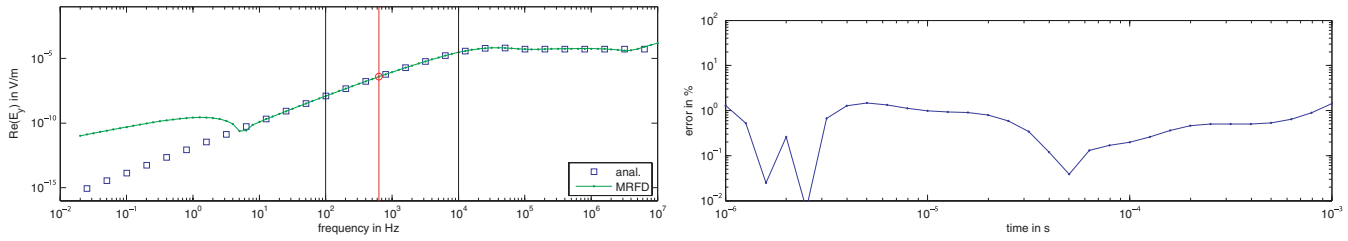

Figure 8. Transfer function and transient error in 3-D layered half-space example using two reference frequencies $f_0 = 10^2$ Hz and $f_0 = 10^4$ Hz used to generate Krylov subspaces of dimension $m = 40$ and 100, respectively. The relative error in the transient is below 1.5 per cent.

at 100 and 150 m away from the source at locations directly over the resistive body.

We observe excellent agreement at early times after current shut-off. At very early times, the response resembles that of a DC source, whereas at late times the response rapidly damps out. We attribute the deviations at late times to the restricted model size which does not correspond to the desired transient time interval.

6 CONCLUSIONS

We have developed an effective algorithm for simulating the electromagnetic field of a transient dipole source. Using a Krylov subspace projection technique, the system of equations arising from the FE discretization of the time-harmonic equation is projected onto a low-dimensional subspace. The resulting system can be solved for a wide range of frequencies with only moderate computational effort. In this way, computing transients using a Fourier transform becomes feasible.

We have carried out numerical experiments for a layered half-space using a 2-D and 3-D FE discretization. By comparing with the analytical solution the MRFD parameters particularly affecting approximation quality, namely domain size, mesh resolution, choice of reference frequency, and dimension of Krylov space, could be adjusted. For large scale 3-D problems the choice of two or more

Downloaded from https://academic.oup.com/gji/article/173/3/766/736358 by U.S. Department of Justice user on 17 August 2022

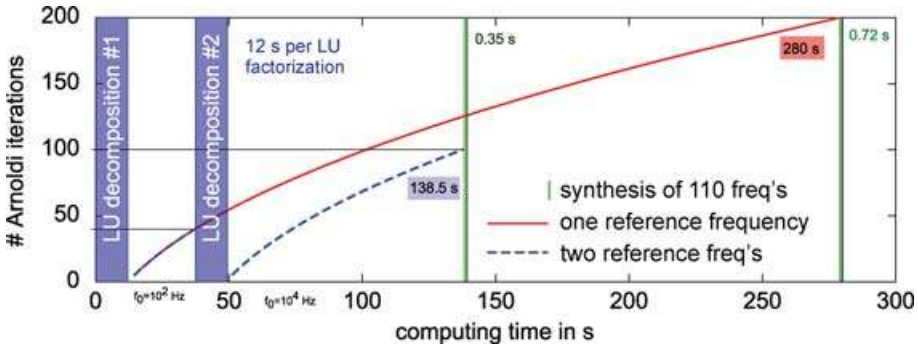

Figure 9. Breakdown of computing time for 3-D layered half-space model for one and two reference frequencies. In the first case one LU factorization is followed by a longer phase of Krylov subspace generation, in the second two LU factorizations are each followed by shorter Krylov phases.

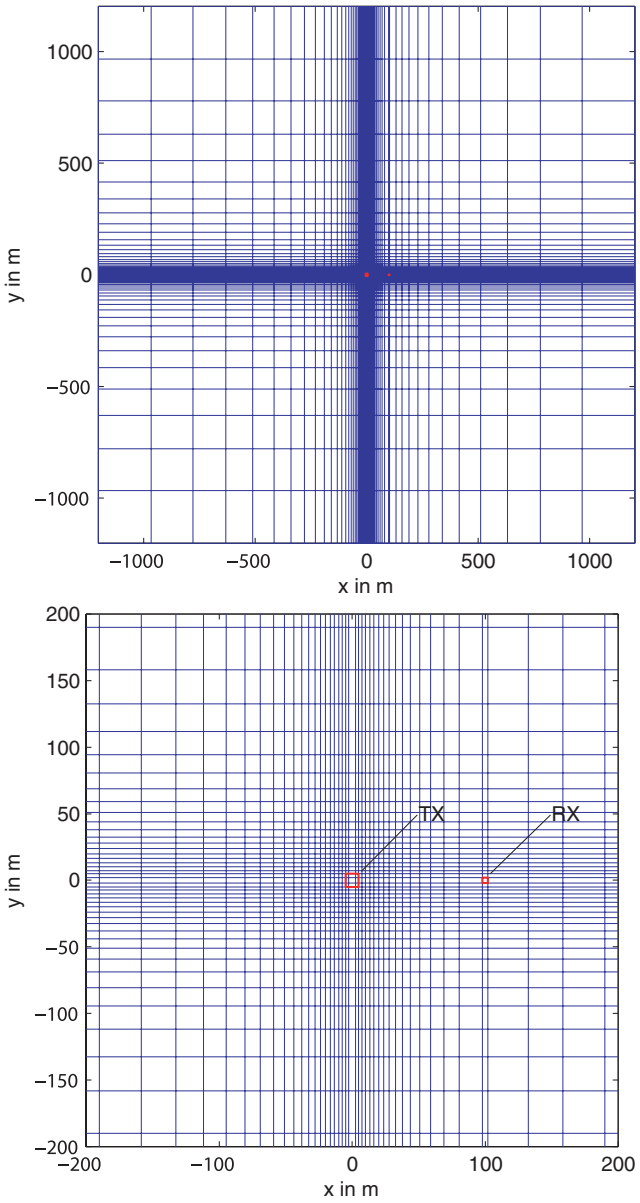

Figure 10. Full extent (a) and excerpt (b) of the finite difference grid (x–y plane, $z = 0$) used for the 3-D layered half-space SLDM calculation.

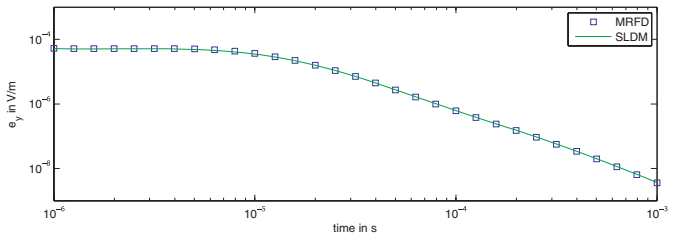

Figure 11. Comparison of transient electric fields e_y at $x = 98$ m obtained by MRFD and SLDM.

reference frequencies further contributes to good agreement between approximate and analytical solution, and saves computing costs at the same time. Comparisons with other established methods as SLDM and FDTD have shown the MRFD method to be in good agreement.

We also emphasize that the FE discretization provides more flexibility with regard to the parametrization of conductivity varations, topography, dipping layers and bathymetry. Adaptive mesh refinement, which is essential for strongly varying gradients in the fields, as well as *a posteriori* error approximation, are also much more easily handled in a FE context.

A further advantage of the frequency domain calculations is that no initial field data are required, as is the case for time domain simulation schemes.

Finally, we mention some possible improvements of the MRFD method: we have chosen the Arnoldi process for generating the Krylov subspace basis, and used a one-sided approximation to approximate the transfer function. A better approximation with a smaller Krylov space can be achieved using two-sided projections and more efficient Krylov subspace basis generation based on the unsymmetric block Lanczos process. Block Krylov methods as well as projection spaces generated by vectors associated with different reference frequencies are another approach to explore. In addition, for very large 3-D calculations the time and memory cost for computing the LU decomposition of the matrix $\mathbf{A}_0$ can become excessive, so that multigrid methods recently developed specifically for the curl–curl operator could replace the linear system solves with $\mathbf{A}_0$ required at each step of the Krylov subspace generation. We will investigate these enhancements in future work.

ACKNOWLEDGMENTS

The authors wish to thank thank Michael Commer (Lawrence Berkeley Laboratories) for the FDTD results, Roland Martin

© 2008 The Authors, *GJI*, **173,** 766–780
Journal compilation © 2008 RAS

Downloaded from https://academic.oup.com/gji/article/173/3/766/736358 by U.S. Department of Justice user on 17 August 2022

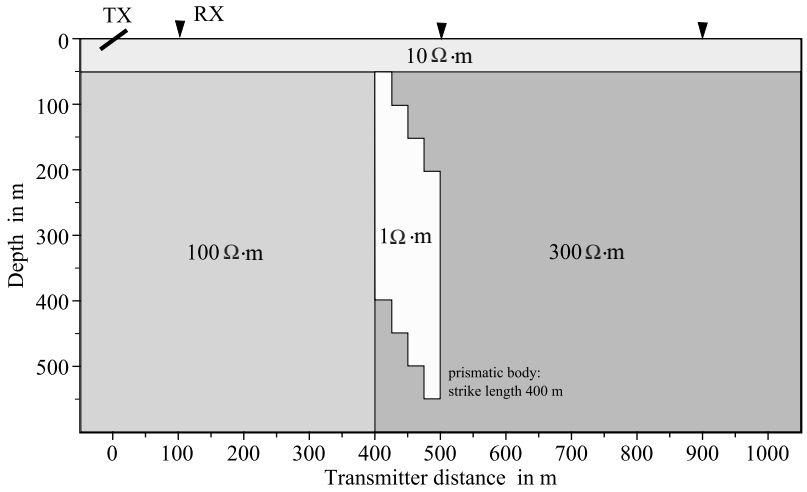

Figure 12. Vertical cross-section of complex 3-D conductivity structure from Commer & Newman (2004).

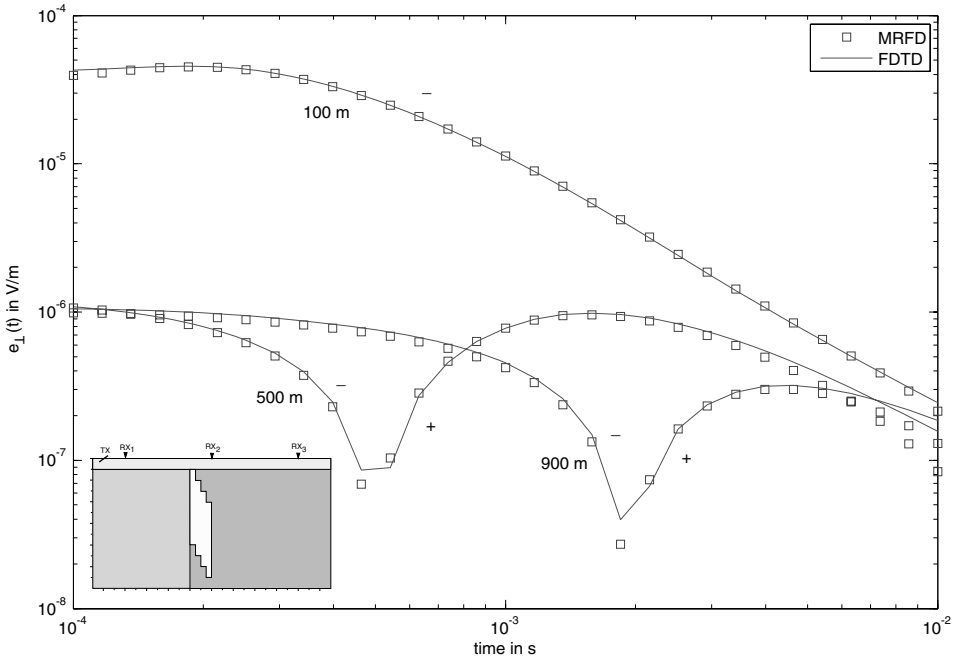

Figure 13. Response of transient electric field $e_{\perp}(t)$ at the receiver positions indicated in Fig. 12 in comparison with the FDTD solution obtained in Commer & Newman (2004).

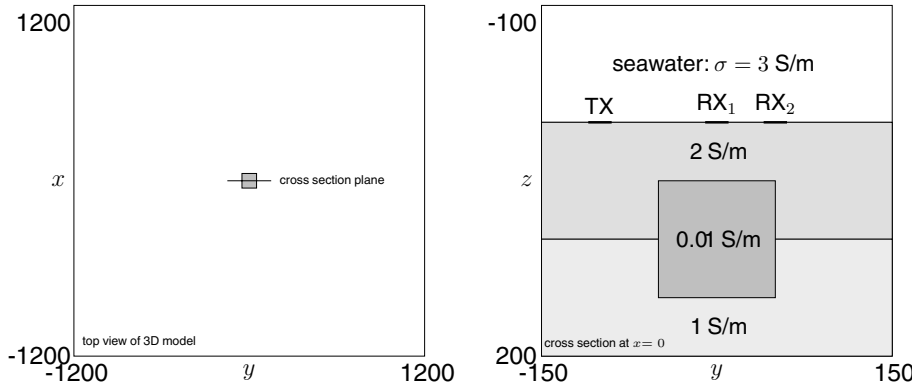

Figure 14. Plane view and vertical cross-section of the conductivity structure of the 3-D marine model. The seawater layer extends up to −1200 m, the seabottom extends down to 1200 m. The transmitter–receiver spacings are 100 and 150 m, respectively.

Downloaded from https://academic.oup.com/gji/article/173/3/766/736358 by U.S. Department of Justice user on 17 August 2022

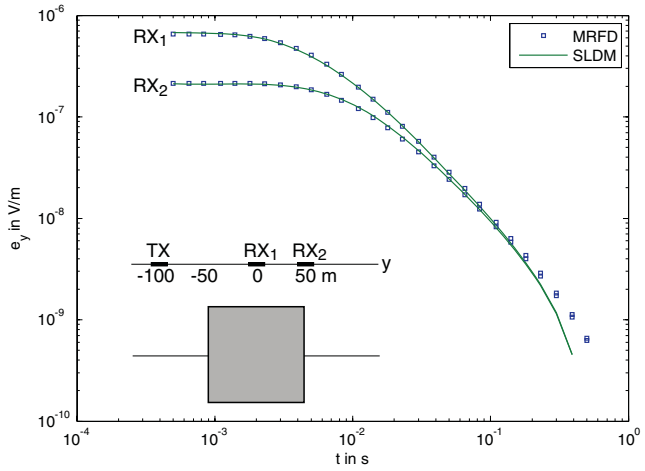

Figure 15. Inline transient electric fields $e_y(t)$ for a current shut-off in comparison with a result obtained by SLDM. Transmitter–receiver spacings are 100 m for RX_1 and 150 m for RX_2.

(University of Cologne) for carrying out comparison calculations with SLDM and Leonid Knizhnerman (Central Geophysical Expedition) for providing access to the SLDMEM3 code. We thank Colin Farquharson and an anonymous reviewer for their thorough reviews and helpful remarks which have improved this manuscript.

REFERENCES

Anderson, W.L., 1979. Numerical integration of related Hankel transforms of orders 0 and 1 by adaptive digital filtering, *Geophysics,* **44,** 1287–1305.

Antoulas, A.C., 2005. *Approximation of Large-Scale Dynamical Systems*, SIAM Publications, Philadelphia, PA.

Aruliah, D. & Ascher, U., 2003. Multigrid preconditioning for Krylov methods for time-harmonic Maxwell's equations in 3D, *SIAM J. Sci. Comput.,* **24**(2), 702–718.

Coggon, J.H., 1971. Electromagnetic and electrical modeling by the finite element method, *Geophysics,* **36**(1), 132–155.

Commer, M. & Newman, G., 2004. A parallel finite-difference approach for 3D transient electromagnetic modeling with galvanic sources, *Geophysics,* **69**(5), 1192–1202.

Druskin, V.L. & Knizhnerman, L.A., 1988. Spectral differential-difference method for numeric solution of three-dimensional nonstationary problems of electric prospecting, *Izvestiya, Earth Phys.,* **24,** 641–648.

Druskin, V.L., Knizhnerman, L.A. & Lee, P., 1999. New spectral Lanczos decomposition method for induction modeling in arbitrary 3-D geometry, *Geophysics,* **64**(3), 701–706.

Edwards, N., 2005. Marine controlled source electromagnetics: principles, methodologies, future commercial applications, *Surv. Geophys.,* **26,** 675–700.

Everett, M. & Edwards, R., 1993. Transient Marine Electromagnetics—the 2.5-D forward problem, *Geophys. J. Int.,* **113**(3), 545–561.

Feldmann, P. & Freund, R.W., 1994. Efficient linear circuit analysis by Padé approximation via the Lanczos process, in *Proceedings of the EURO-DAC '94 with EURO-VHDL '94, Grenoble, France*, pp. 170–175. IEEE Computer Society Press, Los Alamitos, CA.

Freund, R.W., 2003. Model reduction methods based on Krylov subspaces, *Acta Numer.,* **12,** 267–319.

Givoli, D., 1992. *Numerical Methods for Problems in Infinite Domains*,Vol. 33. Elsevier, Amsterdam.

Goldman, M.M. & Stoyer, C.H., 1983. Finite-difference calculations of the transient field of an axially symmetric earth for vertical magnetic dipole excitation, *Geophysics,* **48,** 953–963.

Goldman, Y., Joly, P. & Kern, M., 1989. The electric field in the conductive half space as a model in mining and petroleum engineering, *Math. Method Appl. Sci.,* **11,** 373–401.

Gragg, W.B. & Lindquist, A., 1983. On the partial realization problem, *Linear Algebr. Appl.,* **50,** 277–319.

Greif, C. & Schötzau, D., 2007. Preconditioners for the discretized time-harmonic Maxwell equations in mixed form, *Numer. Linear Algebr. Appl.,* **14**(4), 281–297.

Gupta, P.K., Bennet, L.A. & Raiche, A.P., 1987. Hybrid calculations of three-dimensional electromagnetic response of buried conductors, *Geophysics,* **52**(3), 301–306.

Gupta, P.K., Raiche, A.P. & Sugeng, F., 1989. Three-dimensional time-domain electromagnetic modelling using a compact finite-element frequency-stepping method, *Geophys. J. Int.,* **96**(3), 457–468.

Hiptmair, R. & Xu, J., 2006. Nodal auxiliary space preconditioning in H(curl) and H(div) spaces,Tech. Rep. No. 2006-09. Seminar für Angewandte Mathematik, ETH Zürich.

Jin, J., Zunoubi, M., Donepudi, K.C. & Chew, W.C., 1999. Frequency-domain and time-domain finite-element solution of Maxwell's equations using spectral Lanczos decomposition method, *Comput. Methods Appl. Mech. Engrg.,* **169,** 279–296.

Johansen, H.K. & Sorensen, K., 1979. Fast Hankel Transforms, *Geophys. Prospect.,* **27,** 876–901.

Joly, P., 1989. Pseudo-transparent boundary conditions for the diffusion equation. Part I, *Math. Models Methods Appl. Sci.,* **11,** 725–758.

Lee, K.H., Pridmore, D.F. & Morrison, H.F., 1981. A hybrid three-dimensional electromagnetic modeling scheme, *Geophysics,* **46**(5), 796–805.

Livelybrooks, D., 1993. Program 3Dfeem: a multidimensional electromagnetic finite element model, *Geophys. J. Int.,* **114,** 443–458.

Mitsuhata, Y., 2000. 2-D electromagnetic modeling by finite-element method with a dipole source and topography, *Geophysics,* **65**(2), 465–475.

Monk, P., 2003. *Finite Element Methods for Maxwell's Equations*, Oxford University Press, New York.

Nédélec, J.-C., 1980. Mixed finite elements in $\mathbb{R}^3$, *Numerische Mathematik,* **35,** 315–341.

Nédélec, J.-C., 1986. A new family of mixed finite elements in $\mathbb{R}^3$, *Numerische Mathematik,* **50,** 57–81.

Newman, G.A., Hohmann, G.W. & Anderson, W.L., 1986. Transient electromagnetic response of a three-dimensional body in a layered earth, *Geophysics,* **51,** 1608–1627.

Oristaglio, M.L. & Hohmann, G.W., 1984. Diffusion of electromagnetic fields into a two-dimensional earth: a finite-difference approach, *Geophysics,* **49,** 870–894.

Reitzinger, S. & Schoeberl, J., 2002. An algebraic multigrid method for finite element discretizations with edge elements, *Numer. Linear Algebr. Appl.,* **9**(3), 223–238.

Saad, Y., 1992. Analysis of some Krylov subspace approximations to the matrix exponential operator, *SIAM J. Numer. Anal.,* **29,** 209–228.

Schenk, O. & Gärtner, K., 2004. Solving unsymmetric sparse systems of linear equations with PARDISO, *J. Future Generat. Comput. Syst.,* **20**(3), 475–487.

Schenk, O. & Gärtner, K., 2006. On fast factorization pivoting methods for symmetric indefinite systems, *Elec. Trans. Numer. Anal.,* **23,** 158–179.

Sugeng, F., Raiche, A. & Rijo, L., 1993. Comparing the time-domain EM response of 2-D and elongated 3-D conductors excited by a rectangular loop source, *J. Geomagn. Geoelectr.,* **45**(9), 873–885.

Taflove, A., 1995. *Computational Electrodynamics: The Finite-Difference Time-Domain Method*, Artech House, Norwoord, MA.

Wagner, M.M., Pinsky, P.M., Oberai, A.A. & Malhotra, M., 2003. A Krylov subspace projection method for simultaneous solution of Helmholtz problems at multiple frequencies, *Comput. Methods Appl. Mech. Engrg.,* **192,** 4609–4640.

Wang, T. & Hohmann, G.W., 1993. A finite-difference, time-domain solution for three-dimensional electromagnetic modelling, *Geophysics,* **58,** 797–809.

Downloaded from https://academic.oup.com/gji/article/173/3/766/736358 by U.S. Department of Justice user on 17 August 2022

Ward, S.H. & Hohmann, G.W., 1988. Electromagnetic theory for geophysical applications, in *Electromagnetic Methods in Applied Geophysics*, Chap. 4, ed. Nabighian, M., Soc. Expl. Geoph., Tulsa, Oklahoma, USA.

Yee, K.S., 1966. Numerical solution of initial boundary problems involving Maxwell's equations in isotropic media, *IEEE Trans. Ant. Propag.,* **14,** 302–309.

Downloaded from https://academic.oup.com/gji/article/173/3/766/736358 by U.S. Department of Justice user on 17 August 2022